Vp/Vs distribution in the northern Taiwan area: Implications for the tectonic structures and rock property variations

Jing-Yi Lin [a,*], Shu-Kun Hsu [a], Andrew Tien-Shun Lin [a], Yi-Ching Yeh [b], Chung-Liang Lo [a]

[a] *Department of Earth Sciences, National Central University, 300 Jhongda Road, Jhongli City, Taoyuan County 32001, Taiwan*
[b] *Taiwan Ocean Research Institute, Deep Ocean Exploration Division, Taiwan*

ABSTRACT

The ratio of compressional-wave velocity (Vp) to shear-wave velocity (Vs) is often indicative of lithology and rock conditions. In this study, we determine the Vp/Vs characteristics for the different tectonic features in northern Taiwan and quantify the crack density and saturation by using the OB74 method. The result shows that the highest Vp/Vs values are located beneath the Western Foothills at depths between 4 and 21 km. These Vp/Vs highs are simultaneously characterized by low Vp and low Vs, suggesting the presence of fluids. The average crack density and saturation for each depth can reach as high as 25% and 91% at depths of 7 and 11 km, respectively. This distribution could be caused by the presence of less compacted sediments within the foreland basin and the progressive convergence of crustal faults with depth. As the shallow portion of the foreland basin is highly fractured, fluids could infiltrate into deeper parts to create a highly saturated environment. However, when the depth is deeper than 11 km, the high crack density and saturation area migrate from the west to the east of the Shanchiao Fault. This observation may indicate the presence of a preexisting syn-rift basin buried at depth during the collision. In the Ilan Plain, the highest crack density and saturation are observed in its northeastern portion at a depth of 4 km with values of 17.1% and 60.3%, respectively. However, slightly high saturation values spread throughout the plain at a depth of 15 km, which may indicate a possible fluid conduit from a deep, hot rock body to the surface and could be applied toward studies on geothermal fluid activity.

© 2015 Elsevier B.V. All rights reserved.

1. Introduction

The ratio of compressional-wave velocity (Vp) to shear-wave velocity (Vs) is often indicative of lithology and rock conditions (Domenico, 1984; Eastwood and Castagna, 1983; Kithas, 1976; Miller and Stewart, 1990; Nations, 1974). Based on core measurements, Pickett (1963) obtained Vp/Vs values of 1.9 for limestone dolomite and 1.6 for sandstone. These values have generally been confirmed by subsequent research, which also suggests that mixed lithologies have Vp/Vs values that range between the end members. However, under various temperature and pressure conditions, the Vp/Vs ratio for rocks with different compositions could vary between approximately 1.478 and 2.119, according to Christensen's (1996) experiments. The experiments also showed that higher quartz and feldspar contents result in relatively lower and higher Vp/Vs values, respectively. Generally, the seismic velocity and Vp/Vs values are enhanced with higher pressure. However, the changes are very small, approximately 7.7×10^{-3} per 100 Mpa (Christensen, 1996). In contrast, higher temperature reduces the seismic velocity (Christensen, 1989; Kern and Richter, 1981). Due to the faster decrease

in the Vs with increasing temperature, the Vp/Vs ratio goes up as the temperature rises (Christensen, 1989). Nevertheless, the change in the Vp/Vs ratio with increasing temperature is also very slight, approximately 6.0×10^{-3} per 100 °C (Christensen, 1996; Kern and Richter, 1981). Changes in Vp/Vs values can also be correlated to crack density and fluid saturation. Dry rock, fractured and high crack density areas can result in lower Vp and Vs. Under these conditions, Vp diminishes faster than Vs, and the Vp/Vs ratio decreases (O'Connell and Budiansky, 1974). In contrast, increasing fractures in water-saturated rocks lowers Vp and Vs but raises the Vp/Vs value (Moos and Zoback, 1983; O'Connell and Budiansky, 1974). Thus, these results indicate that higher fluid content increases the Vp/Vs ratio. A Vp/Vs ratio larger than 2 can even occur when partial melting exists in the system. In this case, the reduction in Vs is approximately three times that of Vp (Mavko, 1980). Because fluids do not have a coefficient of rigidity, the Vs changes caused by partial melting and water in the rocks are similar. However, when a rock has the same amount of partial melting or water content, Vp could be different due to the variation in the bulk modulus (Watanabe, 1993). Considering the observations from previous studies, the alternation of Vp/Vs values appears to be more sensitive to the presence of fluid, but less sensitive to changes in temperature and pressure (Christensen, 1996; Christensen and Mooney, 1995; Kern and Richter, 1981).

* Corresponding author at: Department of Earth Sciences, National Central University, 300 Jhongda Road, Jhongli City, Taoyuan County 32001, Taiwan.
E-mail addresses: jylin.gep@gmail.com, jylin@ncu.edu.tw (J.-Y. Lin).

Due to the various characteristics of Vp/Vs variations, numerous studies have been performed for the possible allocation of Vp/Vs analyses in different aspects. Shi et al. (1998) proposed that differential changes in Vp and Vs could be applied to estimate reservoir conditions. Many studies were also performed on volcanic activity analysis based on Vp/Vs variations. Miller and Smith (1999) considered that the presence of partial melting and water would reduce Vs and increase the Vp/Vs values in the Long Valley region, western United States, while Julian et al. (1998) found that gases produced by volcanism in the shallow crust may result in lower Vp/Vs values. In addition, Aggarwal et al. (1973) used Vp/Vs variations for earthquake prediction. Decreasing Vp/Vs that was probably related to the opening of cracks or changes in pore pressure occurred prior to large shocks. Moreover, based on the Vp, Vs and Vp/Vs models in the Kii Peninsula forearc area in Japan, Salah and Zhao (2003) revealed the existence of fluids in the crust and mantle wedge resulting from the dehydration of the subducting Philippine Sea slab, which can explain the observed geophysical and geochemical features in the area.

Changes in the Vp/Vs ratio are sensitive to the presence of fluids, which is very important for seismogenic, geothermal, and geodynamics problems. Clarifying the presence and role of fluids in the geological environment is crucial. Several high resolution seismic tomographic models have been proposed in the Taiwan area (Kim et al., 2005; Kuo-Chen et al., 2012; Lallemand et al., 2001; Lin et al., 2004; Ma et al., 1996; Rau and Wu, 1995; Wu et al., 2009). However, most tectonic interpretations were realized based on variations in Vp. In this study, we determine the Vp/Vs characteristics of different tectonic features in northern Taiwan. Then, the crack density and saturation rate are determined by using the OB74 method (O'Connell and Budiansky, 1974, 1977), which was also used by Zhao and Mizuno (1999) to investigate the source area of the 1995 Kobe earthquake. Finally, some tectonic implications are discussed based on the estimated crack density and saturation data.

2. Geological setting

The island of Taiwan emerged above sea level as a result of the collision of the Philippine Sea Plate (PSP) and Eurasian Plate (EUP) c. 5 Ma (Liu et al., 2000; Teng, 1990). Geologically, Taiwan can be divided into several NNE-SSW trending geological belts (Fig. 1). The western province is associated with the Eurasian continental shelf (Wang et al., 1999) and can be classified into five geological belts (Ho, 1982). They are, from west to east, the Coastal Plain (CP), the Western Foothills (WF), the Hsueshan Ranges (HSR), the Backbond Range (BR) and the East Central Ranges (ECR). These sub-units of the EUP are bounded mainly by faults (Fig. 1). The east-dipping Chuchih Fault (CF) bounds WF from HSR, whereas HSR and BR are separated by the Lishan Fault (LF). Generally, age and metamorphic grade increase to the east. In contrast, the eastern province consists of the Coastal Ranges (CR) and several volcanic islands, which belong to the leading edge of the PSP. The Longitudinal Valley is the suture zone of the EUP and PSP and separates Taiwan into two major tectonic provinces.

The WF province comprises shallow marine to shelf clastic sediments (Teng, 1990) that are essentially unmetamorphosed and imbricated along numerous active folds and thrust faults that trend mainly north or northeast and dip east or southeast (Tillman and Byrne, 1995; Yu et al., 1997). The WF area is considered a classic example of a fold-and-thrust belt that is explained by thin-skinned tectonic models (Clark et al., 1993; Suppe, 1980; Twiss and Moores, 2007). The Hsingchuang Fault was considered to be the westernmost thrust fault in northern Taiwan and the frontal thrust fault of the collisional orogen (Chiu, 1968; Ho, 1982; Ichikawa, 1930). The mountain belt in Taiwan should include the entire region east of the fault (Ho, 1982). In the present day, part of the fault surface was reactivated and transformed into the Shanchiao normal Fault (SF) (Teng et al., 2001; Wang Lee et al., 1978; Wu, 1965), which strikes along the western margin of the Taipei
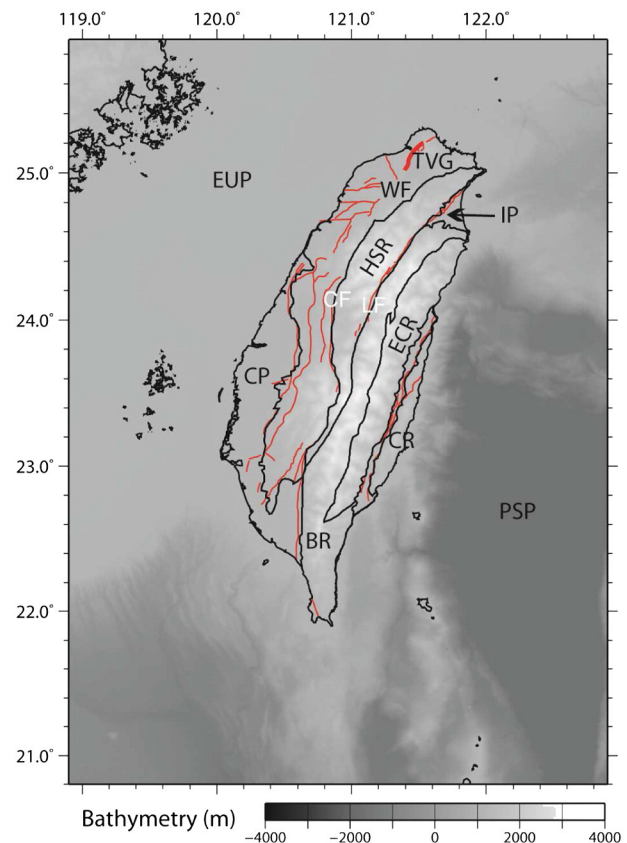
Fig. 1. General geological regions in Taiwan (after Ho (1982)) including the Coastal Plain (CP), Western Foothills (WF), Backbond Range (BR), Eastern Central Range (ECR), Coastal Range (CR), Ilan Plain (IP) and Tatun volcano Group (TVG). EUP and PSP represent the Eurasia Plate and Philippine Sea Plate. Thin red lines show the faults position modified from the website of the Central Geological Survey, MOEA of Taiwan (http://fault.moeacgs.gov.tw/MgFault/Home/pageMap?LFun=3). The thick red line shows the position Shanchiao Fault (SF). LF, Lishan Fault; CF, Chuchih Fault. (For interpretation of the references to color in this figure legend, the reader is referred to the web version of this article.)

Basin. The HSR, the geological unit to the east of the WF, is composed of Tertiary submetamorphic rocks and a pre-Tertiary metamorphic complex. In comparison, the BR's rocks are finer grained and inferred to have been deposited closer to the continental slope than those in the HSR. The ECR exposes rocks with the highest metamorphic grade in the orogen and defines the eastern boundary of the rocks associated with the EUP. Complexes of high grade gneisses and marble have been exposed in the area. In the northernmost part of the WF, the Tatun Volcano Group (TVG) is characterized by andesitic flows that took place during and after the Early Pleistocene orogeny. In northeastern Taiwan, the Ilan Plain (IP) represents the onshore extension of the Okinawa Trough, the back-arc basin associated with subduction at the Ryukyu trench (Teng, 1996).

3. Methods and data

3.1. OB74 method

Using a self-consistent approximation, O'Connell and Budiansky (1974, 1977) proposed the OB74 theory to determine the influence of internal cracks and pores on the elastic properties of rocks. On the assumption that flat circular cracks are aligned randomly in the crust and filled with fluids or air, the crack density (ε) and saturation rate (ξ) can be determined based on the changes in seismic velocity and Vp/Vs. According to OB74, N is the number of micro-pores per unit volume and a is the average radius of the pores. There are N1 dry micro-pores among the N micro-pores, and N2 = N-N1; then, the two

parameters can be expressed as: $\varepsilon = N \times a^3$; $\xi = \frac{N_2}{N}$. Then, the general law for the seismic velocity and the relationships between ε, ξ and Vp/Vs are determined in OB74 and can be described as follows:

$$\frac{\overline{\kappa}}{\kappa} = 1 - \frac{16}{9}\left(\frac{1-\overline{\upsilon}^2}{1-2\overline{\upsilon}}\right)(1-\xi)\varepsilon$$

$$\frac{\overline{G}}{G} = 1 - \frac{32}{45}(1-\overline{\upsilon})\left[1-\xi+\frac{3}{2-\overline{\upsilon}}\right]\varepsilon$$

$$\frac{\overline{E}}{E} = 1 - \frac{16}{45}\left(1-\overline{\upsilon}^2\right)\left[3(1-\xi)+\frac{4}{2-\overline{\upsilon}}\right]\varepsilon$$

$$\frac{\overline{Vs}}{Vs} = \sqrt{\frac{\overline{G}}{G}}$$

$$\frac{\overline{Vp}}{\overline{Vs}} = \sqrt{\frac{(1-\overline{\upsilon})(1-2\upsilon)}{(1-2\overline{\upsilon})(1-\upsilon)}}$$

where K, G, E, υ, Vp, and Vs are the bulk, shear, and Young's modulus, Poisson ratio, and P and S wave velocities for the uncracked volume. $\overline{K}, \overline{G}, \overline{E}, \overline{\upsilon}, \overline{Vp},$ and $\overline{Vs}$ indicate the same quantities for the cracked volume. Please note that the definition of ε is identical to porosity. However, our analyses are performed not only for the normally compacted sediments, but also for the fracture zones. Thus, we suggest the term "crack density" is more appropriate.

3.2. Data

The Vp/Vs values used in this study were obtained from the velocity model of Lin et al. (2004) (Fig. 2b), in which the Vp, Vs and Vp/Vs model was inverted using the arrivals of 3370 earthquakes extracted from the Central Weather Bureau database between December 1990 and May 1999. The seismic wave arrivals used in Lin et al. (2004) are from identical origin to that of the previous studies (e.g. Ma et al., 1996; Rau and

Wu, 1995). However, the method applied for the velocity inversion is different. Even thought different techniques were employed, the Vp distribution obtained from Lin et al. (2004) demonstrates a great consistency with that of Rau and Wu (1995), showing the reliability of the Vp model. In addition, the use of the Simul2000 program (Thurber and Eberhart-Phillips, 1999) in Lin et al. (2004) allows obtaining more reliable Vp/Vs values, which are inverted directly from the time difference between the P- and S-wave arrivals. The "flexible gridding" technique (Thurber and Eberhart-Phillips, 1999) integrated in the program adopts different gridding space intervals in the function of the ray path density. In volumes with high ray path density, the use of fine gridding intervals increases the fine-scale resolution. In regions of poor ray coverage, the values of slave grids are identical to the values of the adjacent master grids. The linkage of slave and master grids helps to recover a reliable smoothed structure in the volumes with low ray path distribution. Therefore, based on these three elements: (1) the high consistency of Vp model with previous study; (2) a more reliable Vp/Vs model inverted directly from the time difference from P- and S-wave; (3) a higher resolution provided by the flexible gridding method, we choose the model of Lin et al. (2004) for our analyses. In the tomographic results of Lin et al. (2004), the Vp and Vp/Vs distributions appear similar (Fig. 2). However, the patterns and depth ranges for the Vp and Vp/Vs anomalies are very different. This comparison shows that a complete tectonic interpretation cannot only depend on the Vp variation, the investigation on the Vp/Vs distribution is also important. The Vp/Vs model of Lin et al. (2004) shows a value range from 1.58 to 1.88 (Fig. 3), which agrees with the global crustal Vp/Vs variations found by previous studies (Zandt and Ammon, 1995). However, shallow depths have bad ray coverage. Thus, only horizontal profiles deeper than 4 km are analyzed.

4. Characteristics for the Vp/Vs distribution

The velocity variance from shallow to deep areas is large. The average Vp varies from 4.80 km/s at 4 km to 8.14 km/s at 60 km. The average Vs alters from 2.81 km/s at 4 km to 4.76 km/s at 60 km. However, the change in the average Vp/Vs value was small, only from 1.70 to 1.73 (Fig. 3). Even thought the Vp and Vs increase significantly with depth,
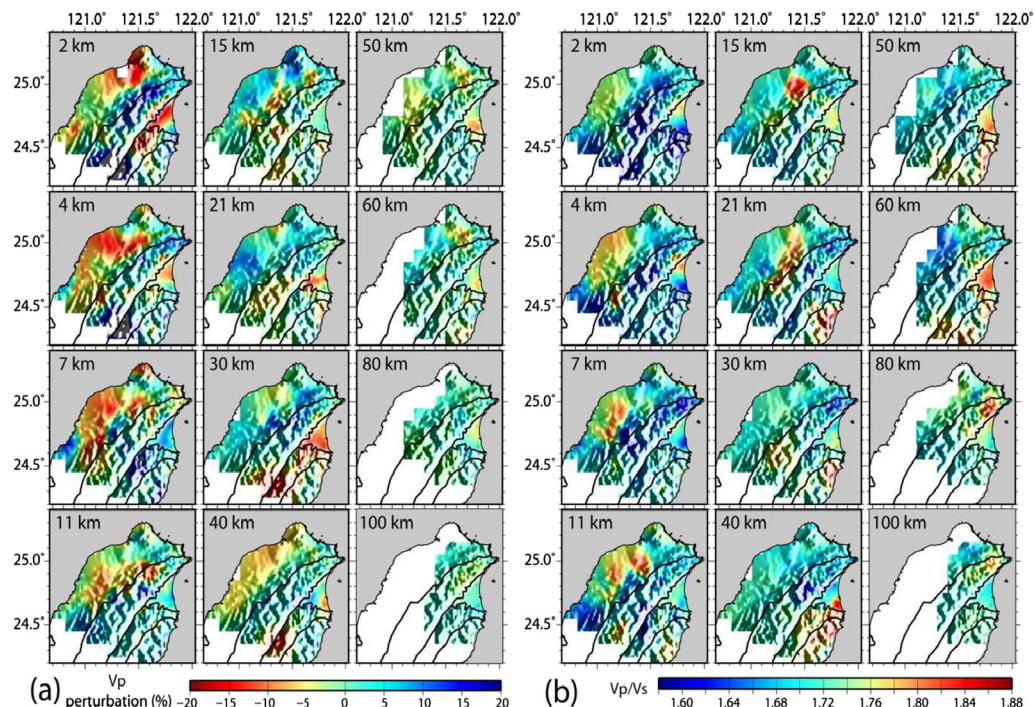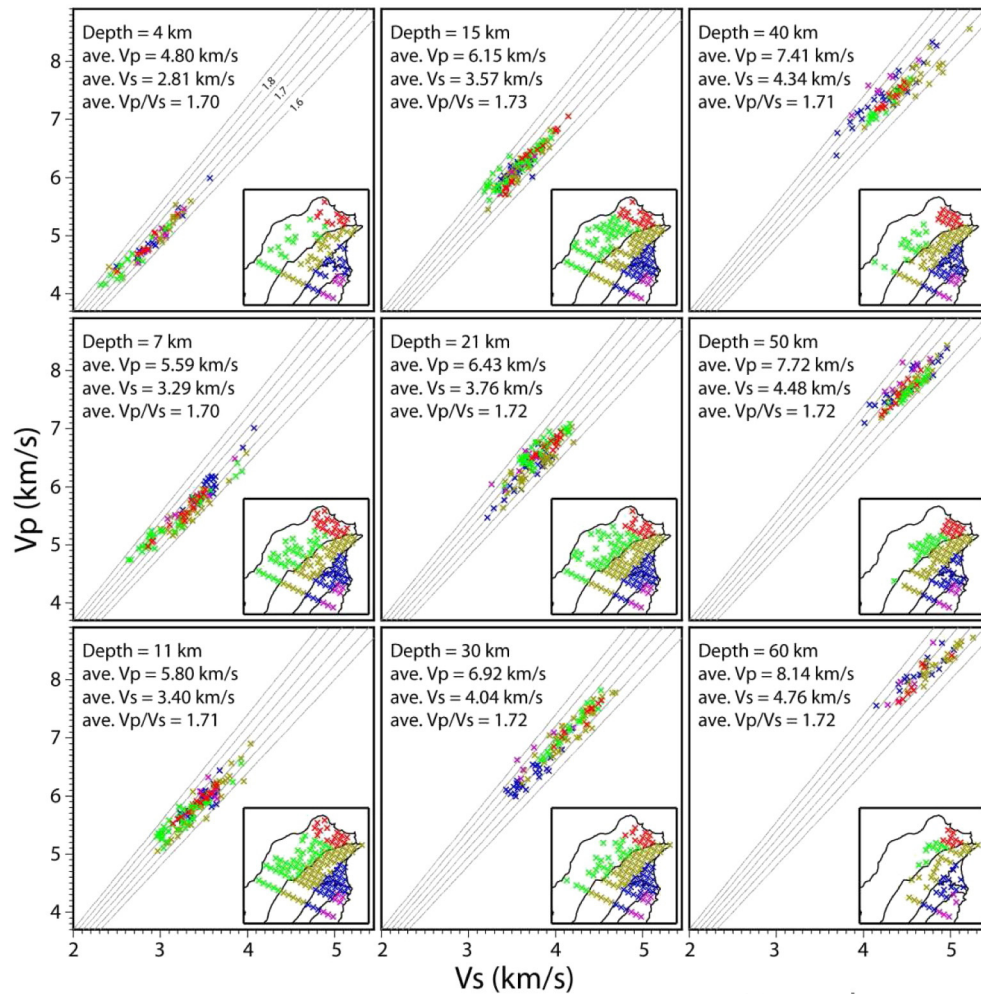

Fig. 2. (a) P-wave and (b) Vp/Vs tomography results displayed for 9 horizontal slices from 4 to 100 km. The black lines represent the geological boundaries.

Fig. 3. Vp–Vs distribution of the tomographic data points. Crosses with different colors show the data points for different geological units. The gray lines show isolines of the Vp/Vs values. The average Vp, Vs and Vp/Vs obtained from the data points at each depth are marked. The inset shows the position of the data points in plan view. (For interpretation of the references to color in this figure legend, the reader is referred to the web version of this article.)

the variation in Vp/Vs reveals little change. This observation suggests that the pressure may increase the seismic wave velocity with depth, but it produces no considerable effect on the Vp/Vs values (Christensen, 1996). The value of Vp/Vs is generally smaller than 1.70 at Earth's surface and becomes slightly larger with a value of 1.72 at deeper depths. The increase in Vp/Vs with depth may reflect differences in the lithological material or increasing plasticity. Although relatively high average Vp/Vs values appear in deep areas, most data points with the largest Vp/Vs values appear at a depth of 15 km in the WF area, with a value larger than 1.80 (Fig. 3).

Based on the tectonic environment, Taiwan has been divided into several geological units. The Vp/Vs distribution of each geological area reveals some slight or distinct differences between them at shallow depths (Fig. 3). For example, the WF area was characterized by relatively lower Vp and Vs at depths shallower than 15 km, whereas the BR has higher Vp and Vs. When the depth is larger than 30 km, the compositions of the different tectonic areas seem to be more homogenous and show a small range of velocities and Vp/Vs variations (Fig. 3). This observation suggests that the classification of geological unit for our data points should be available at the portion shallower than 30 km.

The data points in the WF area are characterized by relatively high Vp/Vs values (green crosses in Fig. 3) when the depth is shallower than 21 km. Although Vp/Vs is high, Vp and Vs show relatively smaller values (Fig. 3), which indicates the presence of fluids (Watanabe, 1993). To the north of the WF, the TVG shows a relatively high seismic velocity and low Vp/Vs compared to the WF area at depths shallower

than 15 km (red crosses in Fig. 3). However, there is almost no difference between the data points in the two areas when the depth is larger than 15 km.

The seismic velocity and Vp/Vs distribution in the HSR, BR and ECR, the three tectonic areas, are similar (brown, blue and purple crosses in Fig. 3). At depths of 21 and 30 km, the data points located in the two easternmost areas of our study area, BR and ECR, show relatively low Vp and low Vs (Fig. 3). When the depth is larger than 30 km, approximately to the depth of the Moho, the two tectonic areas are characterized by high Vp/Vs and low Vs values, which may indicate that partial melting processes occurred near the plate boundary (Lin et al., 2004; Watanabe, 1993).
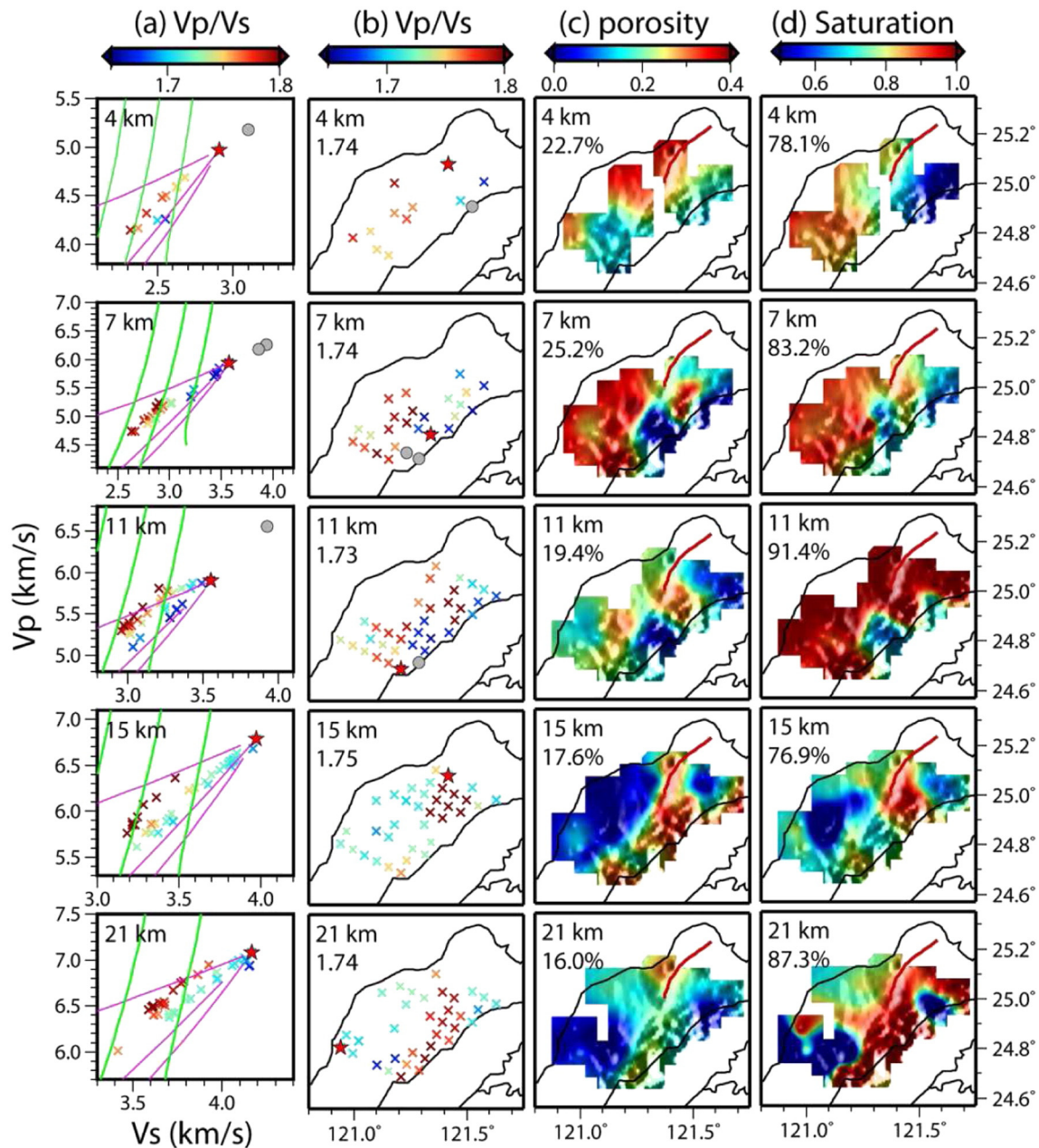
5. Crack density and saturation estimation

Changes in a rock's composition suggest that the basic properties and the velocity of the rock could be different. To decrease the effect caused by different rock compositions, crack density and saturation analyses are only performed for the data located at the same depth and in areas where the geological environment is similar. Moreover, our discussion is restricted to only crustal layers because estimating the values of crack density, saturation and crack density are only valid in the elastic portion (Iverson et al., 1989; O'Connell and Budiansky, 1974). As shown in Fig. 3, for the data points located in the same geological unit, the Vp and Vs are concentrated in a specific range, suggesting the basic component of a geological unit should be identical. Even if

little variance in the rock composition exists, the velocity should still be controlled by a dominated element. Indeed, mineral phase change process may alter suddenly the rock composition as well as the seismic velocity (Kuo-Chen et al., 2012). However, the depths where we applied the analyses are not deep enough to produce this process. It is also true that temperature and pressure could vary at same depth range in inhomogeneous crust. However, their effects are barely significant based on the laboratory experiments (Christensen, 1996; Matsumoto et al., 2010). For example, if the heat flow value at one data point is twice the general considered value, that is 60 °C/km, the temperature at 10 km deep will be 300 °C more than the normal one. According the experiment of Christensen (1996), the corresponding Vp/Vs change for an increase of 300 °C is approximately 1.8×10^{-2}, which cannot even be distinguished on the Vp–Vs distribution (Fig. 3). Similarly, an extra pressure of approximately 260 Mpa, which can be generated by a 5-km thick crust, can induce a change of only approximately 2.0×10^{-2} in Vp/Vs. This value is also too small to be reflected in the estimation of crack density and saturation. Taking into account all these considerations, we suggest that it is executable to neglect the variations induced by the ambient pressure, temperature, and rock properties.

Before the crack density and water saturation are estimated, we have to select a reference velocity for rocks without cracks. Because we cannot know the exact composition of the rock at depth, it is difficult to determine a theoretical velocity value for the reference point in our analyses. However, since the velocity decrease with crack density, the data point with fewer cracks should have relatively higher Vp value. Thus, the reference velocity in our estimation is mainly decided by choosing the largest velocity point in each layer and geological unit.

Fig. 4. Crack density and saturation distribution of the Western Foothills (WF) area. (a) The Vp–Vs distribution of the data points located in the WF. The green and pink lines show the contours for the crack density and saturation, respectively. The values of the crack density contours are 20%, 40% and 60% from right to left; the saturation contours are 0%, 50% and 100% from right to left. (b) The data points in plan view. The red star indicates the reference velocity point. The gray dots show data points with high velocity, which are excluded from the estimation. In (c) and (d), the crack density and saturation distributions are shown; the average values of the data points at each depth and the depth are also marked. The red line shows the position of the SF (Shanchiao Fault). (For interpretation of the references to color in this figure legend, the reader is referred to the web version of this article.)

Nevertheless, this point should be around the upper limit of the velocity group where most data points are located (red star in Figs. 4a, b, 5a and b). Data points that have particularly high velocity and are far from the main velocity group (gray dots in Figs. 4a, b, 5a and b) are excluded from the estimation to avoid the local effect. We found that these relatively high velocity points are located in the boundary of the tectonic unit (Figs. 4b and 5b), which may result from a small imprecise classification of the geological unit. Once the reference velocity is set, the crack density and saturation can be estimated (in Figs. 4 and 5), and the results obtained from each geological unit are described as follows:

5.1. Western Foothills (WF)

In the WF area, the estimated crack density and saturation for each data point are 0%–40% and 50%-more than 100%, respectively (Fig. 4a). The average value of the estimated crack density is between 16.0% and 25.2%. The highest crack density appears at a depth of 7 km and then decreases with depth (Fig. 4c). The average saturation rate is located between 76.9% and 91.4%, and the highest value is observed at a depth of 11 km (Fig. 4d). At depths from 4 to 11 km, the high crack density

and saturation zones appear near the western coast of Taiwan (Fig. 4c and d). However, when the depth becomes deeper than 15 km, the high Vp/Vs, crack density and saturation areas migrate farther east to the western HSR.

5.2. Ilan Plan (IP)

The Ilan plain is located at the junction of two geological zones (HSR and BR), which possess similar velocity distribution patterns (Fig. 3). We estimate the crack density of the Ilan area by using data points from both areas. In this analysis, the highest Vp/Vs values appear to the west of the HSR at a depth of 21 km, which should be affected by the fluid activity in the WF (Fig. 5c and d). Thus, we do not consider this anomalous Vp/Vs as the result of the activity occurring in the IP. Except for the results obtained from 21 km, the average crack density and saturation values are 10.7%–17.9% and 26.7%–64.2%, respectively (Fig. 5c and d). The largest average crack density and saturation occur at depths of 4 km and 15 km. However, the high crack density and saturation zones are concentrated in the northeastern IP at a depth of 4 km, whereas they are spread out across the entire IP at a depth of 15 km.
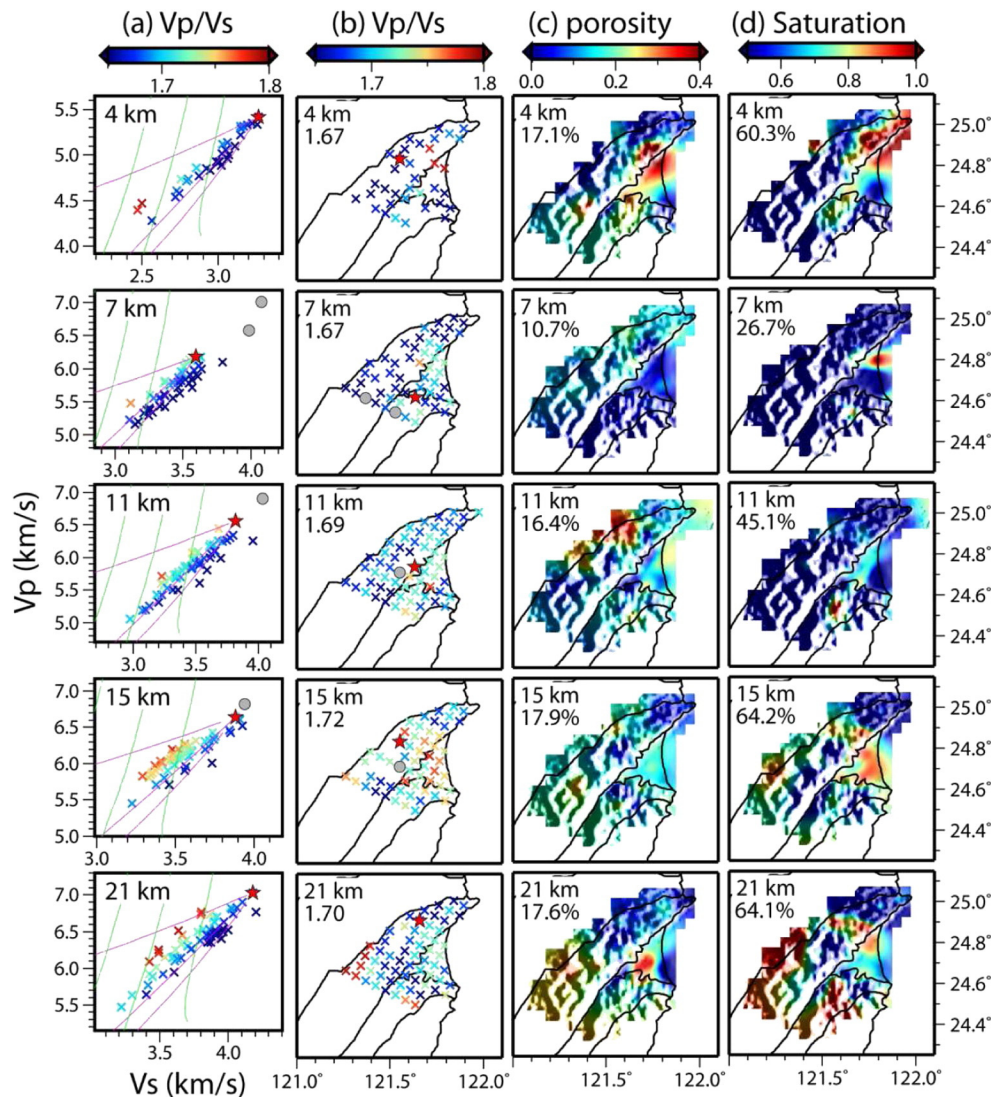
Fig. 5. Crack density and saturation distribution of the Ilan Plain (IP) area. (a) The Vp–Vs distribution of the data points located in the IP. The green and pink lines show the contours for the crack density and saturation, respectively. The values of the crack density contours are 20%, 40% and 60% from right to left; the saturation contours are 0%, 50% and 100% from right to left. (b) The data points in plan view. The red star indicates the reference velocity point. The gray dots show data points with high velocity, which are excluded from the estimation. In (c) and (d), the crack density and saturation distributions are shown; the average values of the data points at each depth and the depth are also marked. (For interpretation of the references to color in this figure legend, the reader is referred to the web version of this article.)

Few high saturation anomalies were observed in the northern IP at a depth of 7 km, and no significant anomalies appeared at a depth of 11 km.

5.3. Tatun Volcano Group (TVG)

The Vp/Vs ratio is 1.70 in the TVG area and does not vary much with depth (Fig. 3). The Vp/Vs value calculated in our study is much lower compared to the average value of approximately 1.823 measured for andesite in the laboratory (Christensen, 1996). Ho (1982) suggested that one major composition of the Tatun Volcano is quartz-rich andesite. The average andesite silica content is approximately 52%, while the silica content of the Tatun Volcano area varies from 50% to 60% (Wang et al., 1999). Thus, an increase in the SiO_2 content decreases Vp/Vs, causing the relatively lower Vp/Vs values in the TVG compared to the averages estimated in similar areas around the world.

Lin (2009) combined two local temporary seismic networks data, the Central Weather Bureau Seismic Network (CWBSN) and the Taiwan Strong Motion Instrumentation Program (TSMIP), to establish a new seismic tomography image for the TVG area. Their result shows the low Vp/Vs and high Vp in the shallow region beneath the TVG, which is consistent with our observation. However, by using a temporal 8-station seismic network deployed from 1996 to 2001, Wen et al. (2012) obtained a high Vp/Vs feature several kilometers wide below the TVG. Because the density of the seismometers in the temporal seismic network was approximately 3 times higher than that of the local network,

we suggest that the scale of the volcanic activity occurring in the TVG area is too small to be resolved by the local seismic network data. Unfortunately, no available relationship between Vp and the percentage of SiO_2 content can be made, and the reference velocity for the OB74 method is impossible to set up. Thus, the crack density and saturation in the TVG could not be determined in this study.

6. Discussion

6.1. High fluid content in northwestern Taiwan

At depths from 4 to 11 km, the high crack density and saturation zones appear near the western coast of Taiwan (Fig. 4c, d, and 6). However, when the depth becomes greater than 15 km, the high Vp/Vs, crack density and saturation areas migrate farther east to the west of the HSR. The boundary where the crack density and saturation distributions change is located along the SF (Figs. 4 and 6). The SF was transformed from part of the Hsingchuang Fault, which was the frontal thrust fault of the collisional orogen. The westward underthrusting rifted margin may result in the presence of different materials on each side of this boundary, namely, foreland sediment to the west (red arrow in Figs. 6b and c) and old, compacted and folded rock to the east (Fig. 6b and c). In addition, the depth of the foreland basin in northwestern Taiwan is located at an approximate depth of 4 to 9 km (Lin et al., 2003). In our result, the highest crack density in the WF was observed at 7 km, located within the foreland basin's sediment layer.
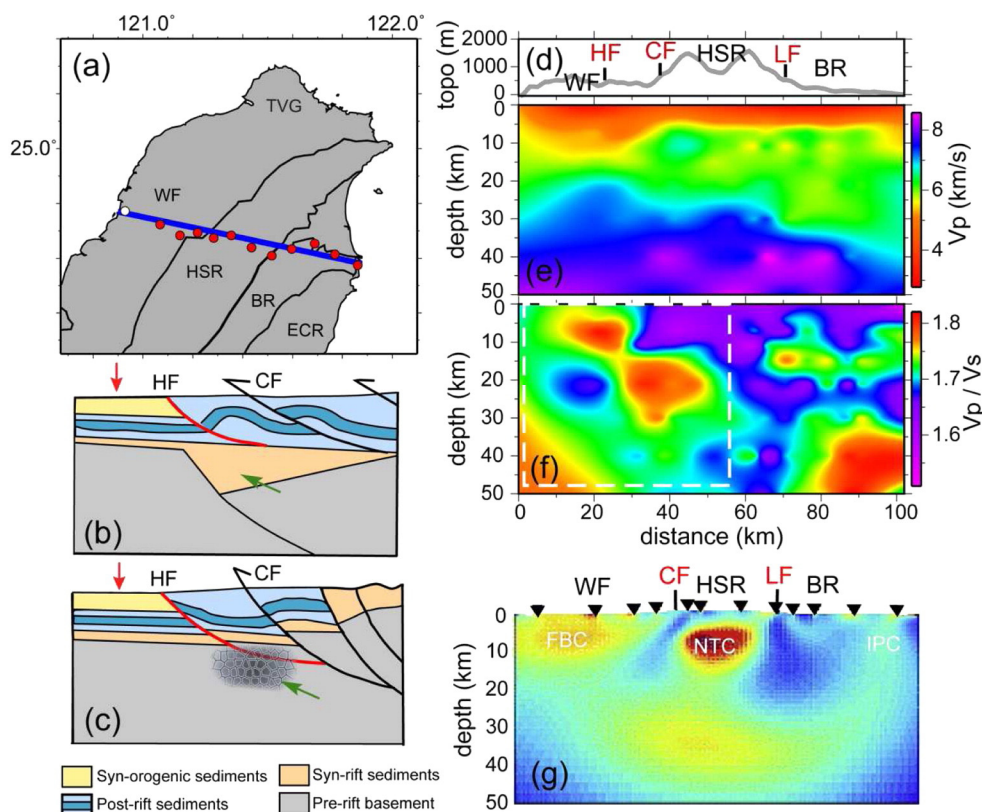
Fig. 6. Resistivity, Vp and Vp/Vs distribution along the magnetotelluric transect across the northern Taiwan in Bertrand et al. (2012). (a) Location map of 12 long-period magnetotelluric data measurements (red circles) along the transect. White circles indicate where only magnetic fields were recorded. Blue line represents the position of the Vp and Vp/Vs cross-section shown in (e) and (f). (b) and (c) are the sketch showing our tectonic interpretation for the NW Taiwan area (white dashed line area in f) based on the Vp/Vs, crack density and saturation distribution. (ab) and (c) illustrate the thin-skinned and thick-skinned model, respectively (modified from Camanni et al. (2014)). In (b), only the sedimentary cover is deformed and the syn-rift basin is preserved beneath the basal detachment. The marine sediment should possess higher crack density and saturation. In (c), the lower crust is involved in the deformation, which may generate some fractures in the deeper part and increase the crack density and saturation (the mosaic area). In both cases, the foreland basin area in the shallow portion of the WF is composed of less compacted sediment in its eastern part, which should have higher crack density. The red and green arrows show the areas where the high crack density and saturation are found in the two models. (d) to (f) are the topographic, Vp and Vp/Vs cross-section along the blue line in (a). (g) represents the resistivity distribution obtained from the magnetotelluric measurements at the stations located in (a) (modified from Bertrand et al., 2012). FBC, NTC and IPC show the location of the foreland basin, northern Taiwan and Ilan Plain conductors mentioned in Bertran et al. (2012). WF, Western Foothills; HSR, Hseuhshan Range; BR, Backbond Range; IP, Ilan Plain; LF, Lishan Fault; CF, Chuchih Fault; HF, Hsingchuang Fault. (For interpretation of the references to color in this figure legend, the reader is referred to the web version of this article.)

Numerous fractures are distributed in western Taiwan (red lines in Fig. 1) and finally converge above or even cut through the rifted margin. The area located just above the basement should possess more fractures and have the highest crack density. Furthermore, due to the distribution of high density faults in the WF area, fluids may not be easily retained in the shallower crustal portion. Thus, the fluids may infiltrate from the shallow portion and concentrate in the deeper part, as demonstrated by the high saturation at a depth of 11 km in our result (Fig. 4).

In contrast, the migration of the high crack density and saturation areas from west to east when the depth is larger than 11 km (Fig. 6a, e and f) could be explained by two possible mechanisms (Fig. 6b and c). First, previous studies suggest that the basal detachment extends from the frontal thrust to the eastern part of the Central Range (thin-skinned model; Malavieille and Trullenque, 2009; Suppe, 1987) (Fig. 6b). In this case, the syn-rift extensional basins, generated during the continental rifting phase, are buried along the basal detachment beneath the underthrusting Taiwan collisional orogen (green arrow in Fig. 6b). Thus, the preexisting syn-rift sediment layer, composed of marine sediment, should have relatively high crack density and saturation. The other mechanism for the migration of the high crack density and saturation areas could be the deformation of the lower crust (green arrow in Fig. 6c). Some other studies showed that the basal detachment, differing from the thin skinned model, does not continue eastward beneath the more internal ranges but ramps down into the lower crust along the western flank of the HSR (thick-skinned model; Brown et al., 2012; Gourley et al., 2007). During the collision process, some fractures may be generated and relatively high crack density and saturation could be produced in the lower crust to the east of the SF if the lower crust is involved with the deformation (green arrow in Fig. 6c). Although both models are possible for the generation of crack density, the first model is preferential because the high crack density area is only limited to the west of the HSR and the involvement of the lower crust in the deformation could not easily explain the high saturation. In addition, the marine sediment that filled the syn-rift basin should have been saturated by sea water, which may explain the extremity high saturation value in the area.

6.2. Geothermal fluid activity in Ilan Plan

Geothermal energy is one of the most important natural resources worldwide. In Taiwan, many studies have revealed that abundant geothermal resources could be stored beneath the IP. The circulation of geothermal fluids within the fracture zone was evidenced by several studies (Lin et al., 2004; Tong et al., 2008). In our result, the highest crack density and saturation are observed at a depth of 4 km in the northeastern portion of the IP and at a depth of 15 km throughout the entire IP. Coincidentally, Lin et al. (2004, 2007) demonstrated that a fluid conduit migrated from the PSP toward the north with increasing depth and arrived at the northeastern part of the IP. This may suggest that the fluid heated by the hot, deep rock body first arrived below the entire IP area at a depth of 21 km and then reached the northeastern IP by following some preferential faults or fractures in the crust. However, there are no obvious crack density and saturation peaks at a depth of 11 km. This observation may indicate a more limited distribution of geothermal fluid activity at this depth range.

6.3. Reliability of the crack density and saturation estimation

Generally, the porosity of compacting sediments follows an exponential trend with depth and may reduce to zero at the brittle–ductile transition (around 10–12 km depth) (e.g. Bahr et al., 2001). In this case, the crack density calculated in our analyses, which has identical definition as porosity, should be extremely overestimated. However, many factors, such as the presence of fractures, the development of grain coats and overpressure effect, could destroy the normal compaction curve and increase the crack density values (e.g. Bloch et al.,

2002; Bowers, 1995; Dunn et al., 1973; Gordon, 1986; Scherer, 1987). For example, a high crack density of 40% was obtained from the C well in the Taiwan Chelungpu-fault Drilling Project (TCDP) at a depth of 1178.7 m and this depth was suspected to be the main fault zone of the 1999 Chi-Chi earthquake (Chen, 2006). Thus, the high crack density estimated in our study may not be impossible.

The pore spaces in underground rocks are mainly saturated with fluid, such as water, oil or gas. If the crakes are filled with gas, the saturation should be lower than 100%. In our studies areas, a few oil reservoirs located in the WF have been exploited, which might explain the lower than 100% saturation values. Volcanic activities could also generate certain amount of gas and fill them in the cracks. Thus, the relatively low saturation estimated in the northern IP might be linked to the presence of volcanic activity in its vicinity area.

Zhao and Mizuno (1999) and Mishra and Zhao (2003) used identical method for the estimation of crack density around the hypocenter of two great earthquakes (1995 M_w 7.2 Kobe earthquake in Japan and 2001 M_w 7.6 Bhui earthquake in western India), the calculated crack density also reach 20% at a depth of approximately 20 km. This value is similar to that one we estimated in the analysis. Moreover, this consistency can also be applied to the saturation distribution. Therefore, our calculation appears to be reliable.

In a tomographic inversion work, the velocity of a grid is obtained from numerous rays passing through a space determined by the gridding size. When the distance between two grids is larger, the velocity model is smoother. The velocity at a specific location is the average of the values possessed by all the surrounding materials. It is true that this "smoothing" or "average" effect might slightly influence the precision of the estimated crack density and saturation values. However, the margin of error should not be large enough to change our interpretation.

6.4. Comparison with magnetotelluric transect

Since most Vp/Vs anomalies in our study are induced by the presence of porosity and fluid which can easily be detected by electromagnetic method, we compare here our result with the resistivity obtained along the magnetotelluric transect across the northern Taiwan (Bertrand et al., 2012) (Fig. 6g). The resistivity inverted from the acquired electromagnetic field shows a low resistivity anomaly of ~5–10 Ω-m within the upper 10 km beneath the WF, so called FBC (Foreland Basin Conductor) in Bertrand et al. (2012)(Fig. 6g), which is in consistency with the high crack density and saturation area demonstrated in our study (Fig. 6f). In addition, near the east coast, a low resistivity of ~25 Ω-m occurs beneath the IP area (IPC, Ilan Plain Conductor), that also coincides with the high crack density and saturation anomalies estimated in our analyses (Fig. 6f and g). Both the FBC and IPC anomalous areas were determined by the Vp/Vs analysis and electromagnetic data and could be explained by fluid filled porosity within the sedimentary rocks. Nevertheless, no corresponding high crack density or saturation is observed to the low resistivity zone located in the northern Central Taiwan, beneath the BR (NTC, Northern Taiwan Conductor) (Fig. 6f and g). The moderate seismic velocity observed in the NTC area (Fig. 6e) could not be explained by the presence of high crack density. Bertrand et al. (2012) suggested that this low resistivity anomaly could be induced by a small percent interconnected porosity saturated with saline fluids. The presence of saline fluids can be reflected by the low resistivity, whereas the small porosity would not be reflected by seismic velocity or Vp/Vs variation. Thus, this interpretation explains the fact that we do not observe this low resistivity area beneath the BR in our study. In consequence, we find a good correlation between the low resistivity and high Vp/Vs value, which suggests the presence of high crack-distributed and high-saturated material. This consistency shows the reliability of the two methods. However, as demonstrated by the result observed in the NTC area, this relationship could break when high conductivity material, such as saline fluid, exists.

7. Conclusions

In this study, we determined the Vp/Vs characteristics of different tectonic features in northern Taiwan and quantified the crack density and saturation by using the OB74 method. The Vp/Vs distributions of each geological area reveal slight or distinct differences between them at shallow depths. When the depth is larger than 30 km, the compositions of the different tectonic areas seem to be more homogenous and show small variations in the velocity and Vp/Vs. At depths of 4–21 km, the highest Vp/Vs values are located beneath the WF. These Vp/Vs peaks are simultaneously characterized by low Vp and Vs, suggesting the presence of fluids. The average estimated crack density and saturation in the WF for each depth can reach 25% and 91%, respectively. At depths shallower than 11 km, the high crack density and saturation areas are located to the west of the SF. This pattern should be due to the presence of less compacted sediment and the high density fault distribution within the foreland basin. The highest crack density appears when all the faults end above or near the base of the foreland basin. As all the fluid cannot be restrained in the high fracture area, the highest saturation appears at a depth of 11 km, in the vicinity of the continental basement. However, the high crack density and saturation areas migrate to the east of the SF when the depth increases. This observation may indicate the presence of a preexisting, rift-related extensional basin that was generated during the continental margin rifting process and has been buried during the collision. In the Ilan Plain (IP), the highest crack density and saturation have been observed at a depth of 4 km with values of 17.1% and 60.3% in its northeastern portion, respectively, where a fluid conduit from a hot, deep rock body was imaged by tomographic methods. However, there are no obvious peaks at a depth of 11 km, which may indicate a more limited distribution of the geothermal fluid activity.

Geological surveys are usually difficult, especially in a mountainous area such as Taiwan. Based on the geophysical method, our study shows that the Vp/Vs ratio is sensitive to the lithological environment and can help geological investigations. Moreover, the perfect consistency between our analyses and the magnetotelluric experiment suggests a large reliability in our method. In consequence, the use of the OB74 does give us an approximate estimation for the crack density and saturation, which could be very important to understand related tectonic or geothermal problems.

Acknowledgements

References

Aggarwal, Y.P., Sykes, L.R., Armbruster, J., Sbar, M.L., 1973. Premonitory changes in seismic velocities and prediction of earthquakes. Nature 241, 101–104.

Bahr, D.B., Hutton, E.W., Syvitski, J.P., Pratson, L.F., 2001. Exponential approximations to compacted sediment porosity profiles. Comput. Geosci. 27, 691–700.

Bertrand, E.A., Unsworth, M.J., Chiang, C.W., Chen, C.S., Chen, C.C., Wu, F.T., Türkoğlu, E., Hsu, H.L., Hill, G.J., 2012. Magnetotelluric imaging beneath the Taiwan orogen: an arc-continent collision. J. Geophys. Res. 117, B01402. http://dx.doi.org/10.1029/2011JB008688.

Bloch, S., Lander, R.H., Bonnell, L., 2002. Anomalously high porosity and permeability in deeply buried sandstone reservoirs: origin and predictability. AAPG Bull. 86, 301–328.

Bowers, G.L., 1995. Pore pressure estimation from velocity data: accounting for overpressure mechanisms besides undercompaction. SPE Drill. Complet. 10, 89–95.

Brown, D., Schimmel, M., Alvarez-Marrón, J., Camanni, G., Wu, Y.-M., 2012. Is there a detachment beneath the Taiwan thrust belt? A view from seismic energy release. Tectonics 31. http://dx.doi.org/10.1029/2012TC003156.

Chen, Z., 2006. Direct Measurements Thermal properties and some related Physical properties from TCDP core Master Thesis, National Central University (75 pp., in Chinese).

Chiu, H.T., 1968. The Hsingchuang Fault in the Taoyuan area, northern Taiwan. Proc. Geol. Soc. Chin. 11, 60–73.

Christensen, N.I., 1989. Reflectivity and seismic properties of the deep continental crust. J. Geophys. Res. 94, 17793–17804.

Christensen, N.I., 1996. Poisson's ratio and crustal seismology. J. Geophys. Res. 101, 3139–3156.

Christensen, N.I., Mooney, W.D., 1995. Seismic velocity structure and composition of the continental crust: a global view. J. Geophys. Res. 100, 9761–9788.

Clark, M.B., Fisher, D.M., Lu, C.Y., Chen, C.H., 1993. Kinematic analyses of the Hsüehshan Range, Taiwan: a large-scale pop-up structure. Tectonics 12, 205–217.

Domenico, S.N., 1984. Rock lithology and porosity determination from shear and compressional wave velocity. Geophysics 49, 1188–1195.

Dunn, D.E., LaFountain, L.J., Jackson, R.E., 1973. Porosity dependence and mechanism of brittle fracture in sandstones. J. Geophys. Res. 78, 2403–2417.

Eastwood, R.L., Castagna, J.P., 1983. Basis for interpretation of Vp/Vs ratios in complex lithologies. SPWLA 24th Annual Logging Symposium. Society of Petrophysicists and Well-Log Analysts.

Gordon, M.J., 1986. Dependence of effective porosity on fracture continuity in fractured media. Groundwater 24, 446–452.

Gourley, J.R., Byrne, T., Chan, Y.-C., Wu, F., Rau, R.-J., 2007. Fault geometries illuminated from seismicity in central Taiwan: implications for crustal scale structural boundaries in the northern Central Range. Tectonophysics 445, 168–185.

Ho, C.-S., 1982. Tectonic Evolution of Taiwan: Explanatory Text of the Tectonic Map of Taiwan. Ministry of Economic Affairs, Republic of China.

Ichikawa, Y., 1930. Explanatory text of the geological map of Taiwan-Toen sheet scale (1: 50,000). Bureau of Productive Industries (Govemment-General of Taiwan) 581, 38.

Iverson, W.P., Fahmy, B.A., Smithson, S.B., 1989. V p V s from mode-converted P-SV reflections. Geophysics 54, 843–852.

Julian, B.R., Pitt, A., Foulger, G., 1998. Seismic image of a CO_2 reservoir beneath a seismically active volcano. Geophys. J. Int. 133, F7–F10.

Kern, H., Richter, A., 1981. Temperature derivatives of compressional and shear-wave velocities in crustal and mantle rocks at 6 kbar confining pressure. J. Geophys. Z. Geophys. 49, 47–56.

Kim, K.-H., Chiu, J.-M., Pujol, J., Chen, K.-C., Huang, B.-S., Yeh, Y.-H., Shen, P., 2005. Three-dimensional VP and VS structural models associated with the active subduction and collision tectonics in the Taiwan region. Geophys. J. Int. 162, 204–220.

Kithas, B., 1976. Lithology, gas detection and rock properties from acoustic logging systems. SPWLA 17th Annual Logging Symposium. Society of Petrophysicists and Well-Log Analysts.

Kuo-Chen, H., Wu, F.T., Roecker, S.W., 2012. Three-dimensional P velocity structures of the lithosphere beneath Taiwan from the analysis of TAIGER and related seismic data sets. J. Geophys. Res. 117. http://dx.doi.org/10.1029/2011JB009108.

Lallemand, S., Font, Y., Bijwaard, H., Kao, H., 2001. New insights on 3-D plates interaction near Taiwan from tomography and tectonic implications. Tectonophysics 335, 229–253.

Lin, Y.-M., 2009. A Study of the Tomography and Seismicity in Taipei Basin and Tatun Volcano Regions, Taiwan and Their Structural Implications Master Thesis, National Taiwan University (103 pp., in Chinese).

Lin, A., Watts, A., Hesselbo, S., 2003. Cenozoic stratigraphy and subsidence history of the South China Sea margin in the Taiwan region. Basin Res. 15, 453–478.

Lin, J.-Y., Hsu, S.-K., Sibuet, J.-C., 2004. Melting features along the western Ryukyu slab edge (northeast Taiwan): tomographic evidence. J. Geophys. Res. 109, B12402. http://dx.doi.org/10.1029/2004JB003260.

Lin, J.-Y., Sibuet, J.-C., Lee, C.-S., Hsu, S.-K., Klingelhoefer, F., 2007. Origin of the southern Okinawa Trough volcanism from detailed seismic tomography. J. Geophys. Res. 112, B08308. http://dx.doi.org/10.1029/2006JB004703.

Liu, T.-K., Chen, Y.-G., Chen, W.-S., Jiang, S.-H., 2000. Rates of cooling and denudation of the Early Penglai Orogeny, Taiwan, as assessed by fission-track constraints. Tectonophysics 320, 69–82.

Ma, K.-F., Wang, J.-H., Zhao, D., 1996. Three-dimensional seismic velocity structure of the crust and uppermost mantle beneath Taiwan. J. Phys. Earth 44, 85–105.

Malavieille, J., Trullenque, G., 2009. Consequences of continental subduction on forearc basin and accretionary wedge deformation in SE Taiwan: insights from analogue modeling. Tectonophysics 466, 377–394.

Matsumoto, Y., Ishikawa, M., Terabayashi, M., Arima, M., 2010. Simultaneous measurements of compressional wave and shear wave velocities, Poisson's ratio, and Vp/Vs under deep crustal pressure and temperature conditions: example of silicified pelitic schist from Ryoke Belt, Southwest Japan. Isl. Arc 19, 30–39.

Mavko, G.M., 1980. Velocity and attenuation in partially molten rocks. J. Geophys. Res. 85, 5173–5189.

Miller, D.S., Smith, R.B., 1999. P and S velocity structure of the Yellowstone volcanic field from local earthquake and controlled-source tomography. J. Geophys. Res. 104, 15105–15121.

Miller, S.L., Stewart, R.R., 1990. Effects of lithology, porosity and shaliness on P-and S-wave velocities from sonic logs. Can. J. Explor. Geophys. 26, 94–103.

Mishra, O., Zhao, D., 2003. Crack density, saturation rate and porosity at the 2001 Bhuj, India, earthquake hypocenter: a fluid-driven earthquake. Earth Planet. Sci. Lett. 212, 393–405.

Moos, D., Zoback, M.D., 1983. In situ studies of velocity in fractured crystalline rocks. J. Geophys. Res. 88, 2345–2358.

Nations, J., 1974. Lithology and porosity from acoustic shear and compressional wave transit time relationships. SPWLA 15th Annual Logging Symposium. Society of Petrophysicists and Well-Log Analysts.

O'Connell, R.J., Budiansky, B., 1974. Seismic velocities in dry and saturated cracked solids. J. Geophys. Res. 79, 5412–5426.

O'Connell, R.J., Budiansky, B., 1977. Viscoelastic properties of fluid-saturated cracked solids. J. Geophys. Res. 82, 5719–5735.

Pickett, G.R., 1963. Acoustic character logs and their applications in formation evaluation. J. Pet. Technol. 15, 659–667.

Rau, R.-J., Wu, F.T., 1995. Tomographic imaging of lithospheric structures under Taiwan. Earth Planet. Sci. Lett. 133, 517–532.

Salah, M.K., Zhao, D., 2003. 3-D seismic structure of Kii Peninsula in southwest Japan: evidence for slab dehydration in the forearc. Tectonophysics 364, 191–213.

Scherer, M., 1987. Parameters influencing porosity in sandstones: a model for sandstone porosity prediction. AAPG Bull. 71, 485–491.

Shi, X., Xia, C., Wu, Y., 1998. The laboratory study on wave velocity under reservoir condition and its affection factors. Acta Geophys. Sin. 41, 234–240.

Shin, T.-C., Chang, C.-H., Pu, H.-C., Lin, H.-W., Leu, P.-L., 2013. The Geophysical Database Management System in Taiwan. Terr. Atmos. Ocean. Sci. 24, 11–18. http://dx.doi.org/10.3319/TAO.2012.09.20.01(T).

Suppe, J., 1980. A retrodeformable cross section of northern Taiwan. Geol. Soc. China Proc. 23, 46–55.

Suppe, J., 1987. The active Taiwan mountain belt. The anatomy of mountain ranges. J. Rodgers 277–293.

Teng, L.S., 1990. Geotectonic evolution of late Cenozoic arc-continent collision in Taiwan. Tectonophysics 183, 57–76.

Teng, L.S., 1996. Extensional collapse of the northern Taiwan mountain belt. Geology 24, 949–952.

Teng, L.S., Lee, C., Peng, C.-H., Chen, W., Chu, C., 2001. Origin and geological evolution of the Taipei basin, northern Taiwan, West. Pac. Earth Sci. 1, 115–142.

Thurber, C., Eberhart-Phillips, D., 1999. Local earthquake tomography with flexible gridding. Comput. Geosci. 25, 809–818.

Tillman, K.S., Byrne, T.B., 1995. Kinematic analysis of the Taiwan slate belt. Tectonics 14, 322–341.

Tong, L.-T., Ouyang, S., Guo, T.-R., Lee, C.-R., Hu, K.-H., Lee, C.-L., Wang, C.-J., 2008. Insight into the geothermal structure in Chingshui, Ilan, Taiwan. Terr. Atmos. Ocean. Sci. 19, 413–424.

Twiss, R., Moores, E., 2007. Struct. Geol.WH Freeman and Company, New York (736 pp.).

Wang Lee, M.W., Cheng, Y.M., Wang, Y., 1978. Geology of the Taipei Basin. Taiwan Mining 30, 79–108.

Wang, K.-L., Chung, S.-L., Chen, C.-H., Shinjo, R., Yang, T.F., Chen, C.-H., 1999. Post-collisional magmatism around northern Taiwan and its relation with opening of the Okinawa Trough. Tectonophysics 308, 363–376.

Watanabe, T., 1993. Effects of water and melt on seismic velocities and their application to characterization of seismic reflectors. Geophys. Res. Lett. 20, 2933–2936.

Wessel, P., Smith, W.H.F., 1998. New improved version of generic mapping tools, EOS. Trans. Am. Geophys. Union 79, 579.

Wen, S., Chang, Y.-Z., Chen, C.-H., Chen, Y.-G., Teng, T.-L., 2012. The seismic velocity and attenuation structure beneath the Tatun volcanic area, Taiwan. J. Asian Earth Sci. 54, 182–191.

Wu, F.T., 1965. Subsidence geology of Hsinchuang structure in the Taipei Basin. Petrol. Geol. Taiwan 4, 271–282.

Wu, Y.-M., Shyu, J.B.H., Chang, C.-H., Zhao, L., Nakamura, M., Hsu, S.-K., 2009. Improved seismic tomography offshore northeastern Taiwan: implications for subduction and collision processes between Taiwan and the southernmost Ryukyu. Geophys. J. Int. 178, 1042–1054.

Yu, S.-B., Chen, H.-Y., Kuo, L.-C., 1997. Velocity field of GPS stations in the Taiwan area. Tectonophysics 274, 41–59.

Zandt, G., Ammon, C.J., 1995. Continental crust composition constrained by measurements of crustal Poisson's ratio. Nature 374, 152–154.

Zhao, D., Mizuno, T., 1999. Crack density and saturation rate in the 1995 Kobe earthquake region. Geophys. Res. Lett. 26, 3213–3216.